organoids

MDPI

Article

Functional Precision Oncology in Rectal Cancer Liver Metastasis: Integrated Genomic and Organoid-Based Drug Sensitivity Profiling

Ebrar Tutar-Torun [1,2], Begüm Kurt [1,2], Dila Sener-Akcora [1,3], Ayse Mine Yilmaz [1,2], Ali Sahin [1,2], Kazım Yalcin Arga [1,4,5], Muharrem Okan Cakir [1,6], Taha Bahsi [7], Mustafa Ozdogan [8] and Betul Karademir-Yilmaz [1,2,9,*]

1 Genetic and Metabolic Disease Research and Investigation Center, Marmara University, Istanbul 34854, Türkiye; ebrartutar99@gmail.com (E.T.-T.); dila.akcora@marmara.edu.tr (D.S.-A.); aysemine.yilmaz@gmail.com (A.M.Y.); alisahin@marmara.edu.tr (A.S.); kyalcinarga@gmail.com (K.Y.A.); m.cakir@kingston.ac.uk (M.O.C.)
2 Department of Biochemistry, School of Medicine, Marmara University, Istanbul 34854, Türkiye
3 Department of Histology and Embryology, School of Medicine, Marmara University, Istanbul 34854, Türkiye
4 Department of Bioengineering, Faculty of Engineering, Marmara University, Istanbul 34854, Türkiye
5 Center for Nanotechnology & Biomaterials Application and Research (NBUAM), Marmara University, Istanbul 34854, Türkiye
6 School of Life Sciences, Pharmacy and Chemistry, Kingston University London, London KT1 2EE, UK
7 Department of Medical Genetics, School of Medicine, Uskudar University, Istanbul 34768, Türkiye; tahabahsi@yahoo.com
8 Division of Medical Oncology, Goztepe Memorial Hospital Cancer Center, Istanbul 34634, Türkiye; ozdoganmd@yahoo.com
9 Department of Biochemistry, School of Medicine, Recep Tayyip Erdogan University, Rize 53100, Türkiye
* Correspondence: betulkarademir@marmara.edu.tr

Abstract

Treatment-refractory rectal cancer liver metastasis represents a major therapeutic challenge, particularly in the absence of actionable genomic biomarkers. Functional precision oncology approaches integrating genomic profiling with patient-derived organoid (PDO) drug testing may provide biologically informed therapeutic prioritization. A 50-year-old female patient with KRAS/TP53-mutant, microsatellite-stable (MSS) rectal adenocarcinoma refractory to FOLFIRINOX was enrolled. A liver metastasis from a treatment-refractory rectal cancer patient was processed to establish three-dimensional patient-derived organoids. Histopathological concordance was assessed using H&E and p53 immunohistochemistry. Comprehensive genomic profiling was performed using a 637-gene targeted next-generation sequencing panel, enabling detection of single-nucleotide variants, indels, copy number variations, microsatellite instability, and tumor mutational burden. Functional drug sensitivity profiling was conducted in parallel 2D and 3D platforms using a customized 17-agent panel, followed by exploratory combinatorial validation. The organoids demonstrated high phenotypic and genomic concordance with the parental tumor, preserving key driver alterations (KRASˆA146T, TP53ˆR175H, APC frameshifts, CCNE1 amplification), microsatellite stability, and low tumor mutational burden (TMB: 6.37 mut/Mb). Functional screening identified selective sensitivity to bevacizumab (IC_{50}: 0.130 µM), doxorubicin (IC_{50}: 0.570 µM), carboplatin (IC_{50}: 0.950 µM), and topotecan (IC_{50}: 1.600 µM) in the 3D organoid model, with consistent cross-platform validation. An exploratory combination assay further supported enhanced viability suppression under bevacizumab-based regimens. Critically, at the time of manuscript preparation, the patient demonstrated radiological disease stabilization under bevacizumab plus trastuzumab deruxtecan, consistent with the organoid-derived response profile. These findings highlight the capacity of integrated

Check for updates

Academic Editor: Cyril Corbet

Received: 31 March 2026
Revised: 14 May 2026
Accepted: 15 May 2026
Published: 21 May 2026

Copyright: © 2026 by the authors. Licensee MDPI, Basel, Switzerland. This article is an open access article distributed under the terms and conditions of the Creative Commons Attribution (CC BY) license.

genomic and organoid-based profiling to uncover therapeutic vulnerabilities beyond standard biomarker assessment. This proof-of-concept case report study demonstrates the feasibility and translational relevance of an established organoid-based functional precision oncology platform for therapeutic prioritization in metastatic rectal cancer.

Keywords: patient-derived organoids; rectal cancer; precision oncology; drug sensitivity profiling; KRAS mutation; liquid biopsy; functional precision oncology

1. Introduction

Rectal cancer remains a significant contributor to global cancer-related morbidity and mortality, distinguished by its unique anatomical, clinical, and biological features [1]. According to GLOBOCAN 2022 estimates, colorectal cancer accounted for approximately 1.93 million new cases and 904,000 deaths worldwide, ranking third in incidence and second in cancer-related mortality globally [2]. Rectal cancer constitutes approximately one-third of all colorectal malignancies, representing a substantial and distinct component of this burden [3]. Economically, colorectal cancer generates considerable strain on healthcare systems; in the United States alone, it was associated with an estimated USD 24.3 billion in annual medical expenditures as of 2020, with metastatic disease disproportionately driving costs [4]. With global incidence projected to increase by up to 60% by 2030—particularly in low- and middle-income countries—the need for more effective therapeutic strategies in advanced disease settings is increasingly urgent [5]. Its localization within the confined space of the pelvis and close proximity to critical urogenital structures make its clinical management particularly challenging [6]. While rectal cancer is historically grouped under colorectal cancer (CRC), increasing evidence supports its characterization as a distinct disease entity, differing from colon cancer in its embryologic origin, venous drainage, microbiome composition, and response to therapy [7,8].

Management of locally advanced rectal cancer typically involves a multimodal approach comprising neoadjuvant chemoradiotherapy (CRT), surgical resection, and adjuvant 5-fluorouracil (5-FU)-based chemotherapy [6]. However, therapeutic responses vary widely. Some patients achieve complete clinical response and may be managed non-operatively, while others show resistance and require radical surgical intervention [9]. The heterogeneity of response reflects underlying tumor biology, particularly in metastatic progression [10].

While the lungs are the most frequent metastatic site in rectal cancer, approximately 20% of cases develop liver metastases, a process that bypasses the portal circulation and engages directly with the systemic vasculature [11]. This distinct route creates a biologically different microenvironment in the liver compared to colon-derived metastases, contributing to greater heterogeneity in molecular signatures, unpredictable drug sensitivities, and variable clinical outcomes [10].

Accurate modeling of this metastatic complexity remains a major limitation of traditional two-dimensional (2D) cell culture systems, which cannot faithfully replicate the intricate tumor-stromal interactions, hypoxic gradients, and immune microenvironment of in vivo tumors. Moreover, these models fail to account for the genetic and epigenetic diversity inherent to patient-derived tumors [9]. Recent advances in high-resolution omics, single-cell sequencing, and ex vivo modeling have enabled more physiologically relevant systems for studying metastatic disease [12].

Among these, three-dimensional (3D) patient derived organoid (PDO) models have emerged as powerful tools capable of preserving the cellular heterogeneity, genomic landscape, and phenotypic characteristics of the original tumor tissue. Organoids derived from

rectal cancer, both from primary lesions and metastatic sites such as the liver, provide a versatile platform for drug screening, biomarker discovery, and therapeutic response prediction [13]. Typically embedded in Matrigel-based scaffolds and cultured with essential growth factors such as EGF, Noggin, and R-spondin, these organoid systems support sustained proliferation and maintain tissue architecture. Importantly, they offer clinically relevant data while reducing dependence on animal models, and their high concordance with original tumor genomics reinforces their utility in precision oncology [14].

In the present study, we establish and functionally characterize a patient-derived organoid model generated from a rectal cancer liver metastasis and integrate comprehensive genomic profiling with ex vivo drug sensitivity testing. Beyond modeling this individual metastatic lesion, the workflow applied here represents part of an established functional precision oncology platform in our laboratory, designed to enable real-time therapeutic prioritization in solid tumors. By integrating histopathological validation, genomic profiling, and functional drug testing, this study illustrates how organoid-based precision oncology can inform therapeutic decision-making in treatment-refractory rectal cancer.

2. Materials and Methods

2.1. Patient Sample and Platform Integration

A 50-year-old female was diagnosed with moderately to poorly differentiated rectal adenocarcinoma following evaluation for lower abdominal discomfort and intermittent rectal bleeding. Colonoscopic biopsy confirmed rectal malignancy, and cross-sectional imaging demonstrated synchronous liver metastases. Core needle biopsy of the hepatic lesion confirmed metastatic adenocarcinoma consistent with rectal origin.

Immunohistochemical profiling revealed CK7 positivity with CK20 and CDX2 negativity. Although CK7 expression is atypical for colorectal primaries, it has been reported in a subset of rectal cancers, particularly those with mucinous differentiation [15]. The Ki-67 proliferation index was approximately 40–50%, and diffuse nuclear p53 positivity was observed. No lymphovascular or perineural invasion was identified, and surgical margins were negative.

Comprehensive molecular profiling of formalin-fixed paraffin-embedded tumor tissue identified a pathogenic KRAS p.A146T mutation and TP53 p.R175H hotspot mutation, along with two APC frameshift variants (c.1620dupA; c.4455delT) and concurrent APC amplification. No alterations were detected in BRAF, NRAS, or mismatch repair genes. The tumor was microsatellite stable (MSS) with a tumor mutational burden of 6.59 mutations/Mb and minimal PD-L1 expression (<1% tumor cells), indicating limited eligibility for immune checkpoint inhibition.

The patient exhibited no significant clinical or radiological response to first-line FOLFIRINOX chemotherapy. Given the presence of KRAS mutation-associated resistance to anti-EGFR therapy and the absence of actionable immunotherapy biomarkers, therapeutic options were limited.

Fresh liver metastasis tissue was obtained during surgical resection and transferred under controlled hypothermic conditions (4 °C) to Marmara University for integrative analysis within our established organoid-based functional precision oncology platform. This platform standardizes tumor dissociation, three-dimensional organoid expansion, genomic profiling, and high-throughput drug sensitivity testing under a unified translational workflow designed to enable therapeutic prioritization in biomarker-limited solid tumors.

Written informed consent for research use of tumor tissue was obtained in accordance with the Declaration of Helsinki, and the study protocol was approved by the Marmara University Institutional Ethics Committee (Approval No: 26-0250; Date: 20 February 2026).

2.2. Tumor Dissociation and Organoid Establishment

Fresh liver metastasis tissue was transported at 4 °C in tissue preservation solution and processed within 12 h of surgical resection. Upon arrival, the specimen was partitioned for histological evaluation, molecular profiling, and organoid establishment (Figure 1).

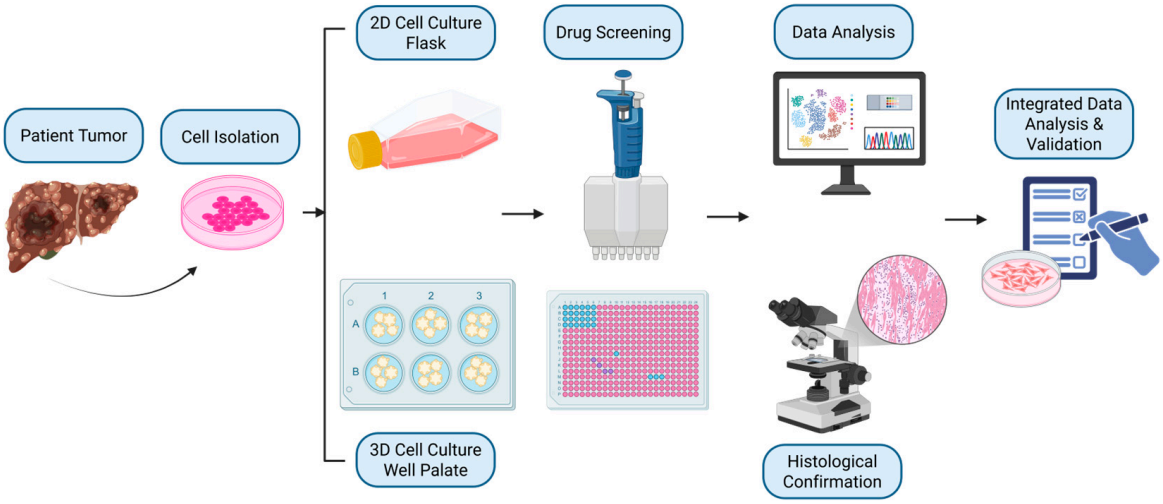

Figure 1. Experimental workflow for patient-derived tumor modeling and multimodal validation. A biopsy specimen was obtained from the patient's hepatic lesion, followed by tumor cell isolation and establishment of parallel 2D monolayer and 3D organoid cultures. Both model systems were subsequently subjected to high-throughput drug screening. Key findings were corroborated by genomic profiling (DNA sequencing; DNA-seq) and histopathological validation, including hematoxylin and eosin (H&E) and p53 immunohistochemistry, enabling integrated interpretation of pharmacologic response with molecular and tissue-level features.

Tumor tissue designated for organoid culture was mechanically and enzymatically dissociated using a standardized tumor dissociation protocol (see Supplementary Methods). Following filtration and centrifugation, viable cells were quantified by Trypan Blue exclusion. Only preparations with viability exceeding 70% were proceeded to culture establishment.

For 2D cultures, primary cells were seeded at a density of 1×10^5 cells/cm^2 in DMEM/F12 (supplemented with 10% fetal bovine serum (FBS) and 1% penicillin-streptomycin and expanded under standard conditions (37 °C, 5% CO_2).

For 3D culture, dissociated cells were established using two parallel methods: ultra-low attachment (ULA) flask culture and Matrigel dome embedding. In the ULA condition, cells were seeded at 2×10^5 cells/cm^2 in defined organoid medium (Advanced DMEM/F12 base; serum-free) organoid medium supplemented with EGF, FGF2, R-spondin, A83-01, nicotinamide, N-acetylcysteine, and B27/N2 additives. For Matrigel dome culture, dissociated cells were resuspended in growth factor-reduced Matrigel at 1.0×10^4 cells per droplet and overlaid with the same organoid medium following gelation. Organoids were maintained for 14–21 days with medium replacement every 2–3 days. Morphological development was monitored by bright-field microscopy.

Detailed composition of media, enzyme concentrations, incubation conditions, and seeding parameters are provided in Supplementary Methods (Table S1).

2.3. Histological Analyses of Original Tumors and Organoids

Rectal cancer tissues and patient-derived organoids were fixed in 10% neutral buffered formalin at room temperature. Organoids were transferred into 1 mL Eppendorf tubes, mixed with 0.5% agarose gel, and solidified overnight at 4 °C. Agarose-embedded organoid molds were then transferred to tissue cassettes. Subsequently, both primary tissues and

organoids were subjected to routine tissue processing and embedded in paraffin as previously described [16]. Sections of 4–5 μm thickness were stained with hematoxylin and eosin (H&E) for histopathological examination. Immunohistochemistry (IHC) was performed with the indirect immunoperoxidase method. p53 anti-human primary antibody (1:100, Clone DO-7, lot: 41654182, Dako Omnis, Agilent Technologies, Santa Clara, CA, USA) was utilized to monitor nuclear positivity. Slides were examined and photographed using an Olympus BX51 microscope equipped with an Olympus DP 72 digital camera (Tokyo, Japan).

2.4. Two-Dimensional and 3D Cell Seeding for Drug Screening

For 2D drug sensitivity assays, primary tumor-derived cells were expanded under standard culture conditions for 14 days and seeded into 384-well clear flat-bottom TC-treated polystyrene plates at a density of 1.0×10^3 cells per well (25 μL per well). After 24 h of attachment, cells were exposed to serial drug concentrations for 48 h prior to viability assessment.

For 3D assays, mature organoids were enzymatically dissociated into single cells and reseeded into 384-well ultra-low attachment black/clear-bottom plates at 1.0×10^3 cells per well in organoid medium combined with growth factor-reduced Matrigel at a 97:3 volumetric ratio (25 μL per well), in organoid medium supplemented with extracellular matrix support. Following a 6-day recovery period allowing spheroid reformation, drug treatments were administered across multiple concentrations. Viability was quantified after 6 days of exposure.

Detailed procedures including passage number at the time of assay (passage 1–2 for both 2D and 3D cultures), enzymatic dissociation conditions, plate formats, incubation times, and reagent specifications are provided in Supplementary Methods.

2.5. Functional Drug Sensitivity Profiling

High-throughput drug screening was performed in parallel 2D monolayer cultures and 3D organoid platforms using a customized 17-agent panel incorporating cytotoxic, targeted, and anti-angiogenic compounds.

Cells and organoids were seeded in 384-well plates under standardized density conditions. Drug stock solutions were prepared at 10 mM in dimethyl sulfoxide (DMSO) and serially diluted two-fold across eight concentration points spanning 0.001–10 μM in the respective culture medium; the final DMSO concentration in all wells did not exceed 0.1% (v/v). Drug exposure occurred across four concentrations per agent, and viability was quantified using WST-1 (Roche Diagnostics GmbH, Mannheim, Germany) (2D; 48 h exposure, absorbance at 450 nm) and ATP-based luminescence (CellTiter-Glo®, (Promega, PRG9681, Madison, WI, USA) 3D; 6-day exposure, luminescence normalized to vehicle-treated controls).

Dose–response curves were generated using four-parameter logistic (4PL) non-linear regression in GraphPad Prism 7.0b. Goodness-of-fit was evaluated by R^2 values; curves with $R^2 < 0.90$ were excluded from IC_{50} determination. Agents for which ≥50% inhibition was not achieved within the tested concentration range were designated IC_{50} = not determinable (N.D.). IC_{50} values were calculated and interpreted in the context of literature benchmarks and ongoing clinical studies.

All assays were performed with three technical replicates per concentration point. It should be noted that, given the single-patient proof-of-concept nature of this study, independent biological replicates from separate organoid passages were not feasible; accordingly, all reported variability reflects technical rather than biological replicate variance. Results

are expressed as mean ± standard deviation (SD) of three technical replicates relative to vehicle-treated controls (set to 100%).

A weighted prioritization algorithm incorporating drug potency, sensitivity classification, and clinical approval status was applied to rank candidate therapies. Briefly, each compound was scored across three dimensions: (i) IC_{50} magnitude relative to published preclinical reference values (Sensitive: below reference range; Low Sensitive: within reference range; Not Sensitive: above reference range or N.D.); (ii) clinical approval status for the relevant indication (approved: +2, investigational: +1, not approved: 0); and (iii) genomic concordance with the patient's molecular profile (supported: +1, neutral: 0, contraindicated: −1). Composite scores were summed and used to rank candidate therapies in descending order of translational priority.

2.6. Validation of Next-Generation ADC Efficacy: Combinatorial Drug Screening

Given the organoid's sensitivity to topoisomerase I inhibitors (e.g., Topotecan) observed in the initial screening, we sought to evaluate the efficacy of Trastuzumab Deruxtecan (T-DXd), a HER2-targeting antibody–drug conjugate with a topoisomerase I inhibitor payload. To validate the potential clinical utility of this agent in combination with anti-angiogenic therapy, a supplementary ex vivo assay was designed. Organoids derived from the liver metastasis were seeded into 384-well plates. During the evaluation of bevacizumab efficacy in 3D cell culture, VEGF was added to the culture medium. Bevacizumab was applied at a fixed concentration corresponding to its previously determined IC_{50} value (0.130 μM). Trastuzumab Deruxtecan (T-DXd) was administered at varying concentrations ranging from 0.001 μM to 10 μM in the presence of the fixed Bevacizumab dose. Additionally, T-DXd was tested as a single agent across the same concentration range. Cell viability was assessed after 6 days using the CellTiter-Glo®, (Promega, PRG9681, Madison, WI, USA) Luminescent Cell Viability Assay (ATP-based), and results are expressed as mean ± SD of three technical replicates and dose–response curves were generated to analyze combinatorial efficacy and fixed-dose combination activity, without formal synergy modeling.

2.7. DNA Targeted Analysis of Original Tumor and Organoids

Genomic DNA from organoid cultures was extracted using the QIAamp DNA Mini Kit (Cat/ID: 56304, QIAGEN, Hilden, Germany) according to the manufacturer's protocol. Organoids were cultured in Ultra-Low Attachment 25 cm^2 flasks prior to DNA isolation. DNA sequencing data of the original tumor tissue were obtained from previously conducted clinical tests (Prime DX, Genekor, Gerakas, Greece), and the accuracy of those results was accepted as valid for comparative analysis. The purity and concentration of the extracted organoid DNA were assessed using a NanoDrop 2000 spectrophotometer and a Qubit 2.0 fluorometer (Life Technologies' second-generation, Carlsbad, CA, USA) (Catalog no. Q32866, respectively. Genomic profiling of the patient-derived organoid was conducted using the NanOnco Plus Panel v3.0 (NanodigmDx, China). In total, 637 genes spanning approximately 2.4 Mb of the human genome were analyzed, enabling simultaneous detection of single-nucleotide variants (SNVs), small insertions/deletions (indels), copy number variations (CNVs), gene rearrangements, and microsatellite instability (MSI). Sequencing was performed on the MGI DNBSEQ-T7 platform (MGI Tech Co., Shenzhen, China) using 100 bp paired-end reads. Raw image files were processed with MGI Base Calling Software V 2.x, and FASTQ files were generated for downstream analysis. The mean on-target coverage depth exceeded 5000× for organoid samples, ensuring high sensitivity for somatic variant detection.

2.8. Bioinformatics Analysis

Adaptor trimming and quality filtering were carried out using fastp (v0.23.2). Clean reads were aligned to the human reference genome (GRCh37/hg19) with Burrows-Wheeler Aligner (BWA-MEM, v0.7.12). Local realignment around indels and base-quality recalibration were performed using GATK (v3.8), and PCR duplicates were marked with Picard tools. Somatic SNVs and indels were called with VarScan2 (v2.4.2) under the following parameters: minimum coverage 100×, minimum variant allele frequency (VAF) 5%, and $p < 0.05$ (Fisher's exact test). Copy number variations (CNVs) were inferred from normalized read depth and log2 copy-ratio values using an in-house algorithm based on CNVkit (v0.9.9). Microsatellite instability (MSI) status was calculated from the targeted microsatellite loci included in the panel; samples with an MSI score < 20% were classified as microsatellite stable (MSS). Tumor Mutational Burden (TMB) was determined as the number of somatic, non-synonymous mutations per megabase (mut/Mb) within the targeted region. Variant annotation was performed using ANNOVAR (v5.2.3), ClinVar, COSMIC v98, and CIViC (v2.7.2), following ACMG/AMP guidelines for variant classification.

Genomic concordance between the tumor and organoid samples was assessed by comparing somatic variant lists and CNV profiles. Mutations shared between both samples were classified as clonally conserved, whereas variants unique to either the tumor or organoid were considered subclonal or culture acquired. Copy-number correlation was evaluated across all targeted loci, and genome-wide CNV plot were generated to visualize amplification and deletion events (Figure S1).

3. Results

3.1. Morphological Validation of Patient-Derived Organoids

Primary tumor cells successfully expanded in both 2D monolayer and 3D culture systems following dissociation of liver metastatic tissue (Figure 2). In 2D conditions, cells displayed adherent epithelial morphology with irregular polygonal contours and variable cytoplasmic density (Figure 2A). In contrast, 3D culture under ultra-low attachment and Matrigel-supported conditions enabled progressive cellular aggregation and spherical self-organization (Figure 2B).

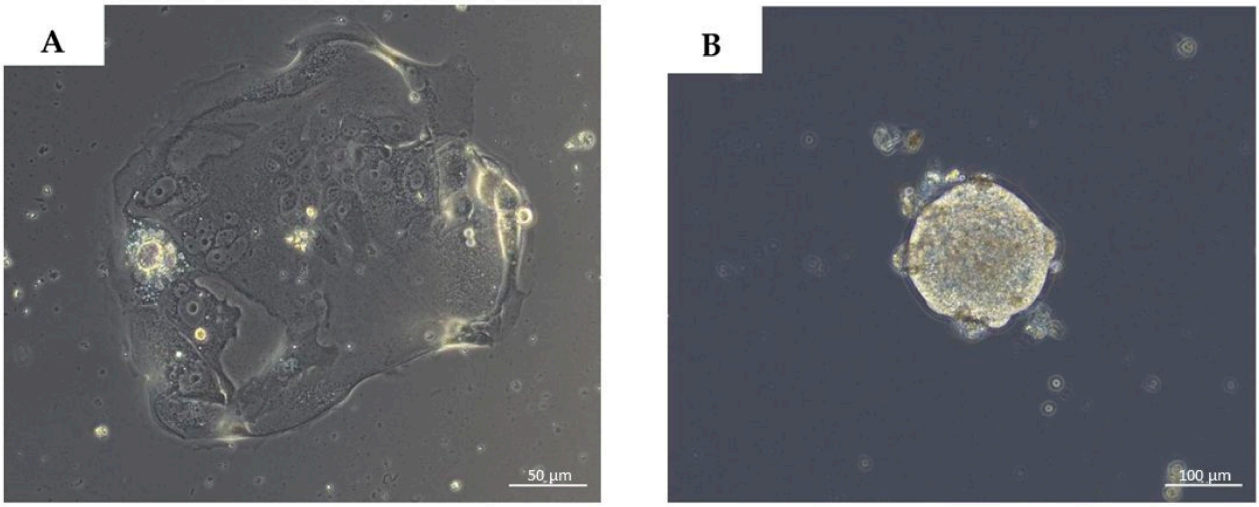

Figure 2. Representative bright-field images of patient-derived cultures established from a rectal-origin liver metastasis. (**A**) 2D monolayer culture in a T25 flask. Scale bar: 50 µm; objective magnification: 40×. (**B**) Matrix-free 3D spheroid-like structure formed in an Ultra-Low Attachment (ULA) T25 flask using the study-specific organoid medium (Scale bar = 100 µm; 20× objective).

Time-course analysis demonstrated structural maturation of organoids over a 14-day period (Figure 3). By day 7, compact multicellular aggregates were evident, with early lumen-like structures observed in some spheroids. By day 14, organoids exhibited increased size, enhanced cellular density, and more defined architectural organization, including peripheral viable cell layers and central compact regions suggestive of in vivo-like growth dynamics.

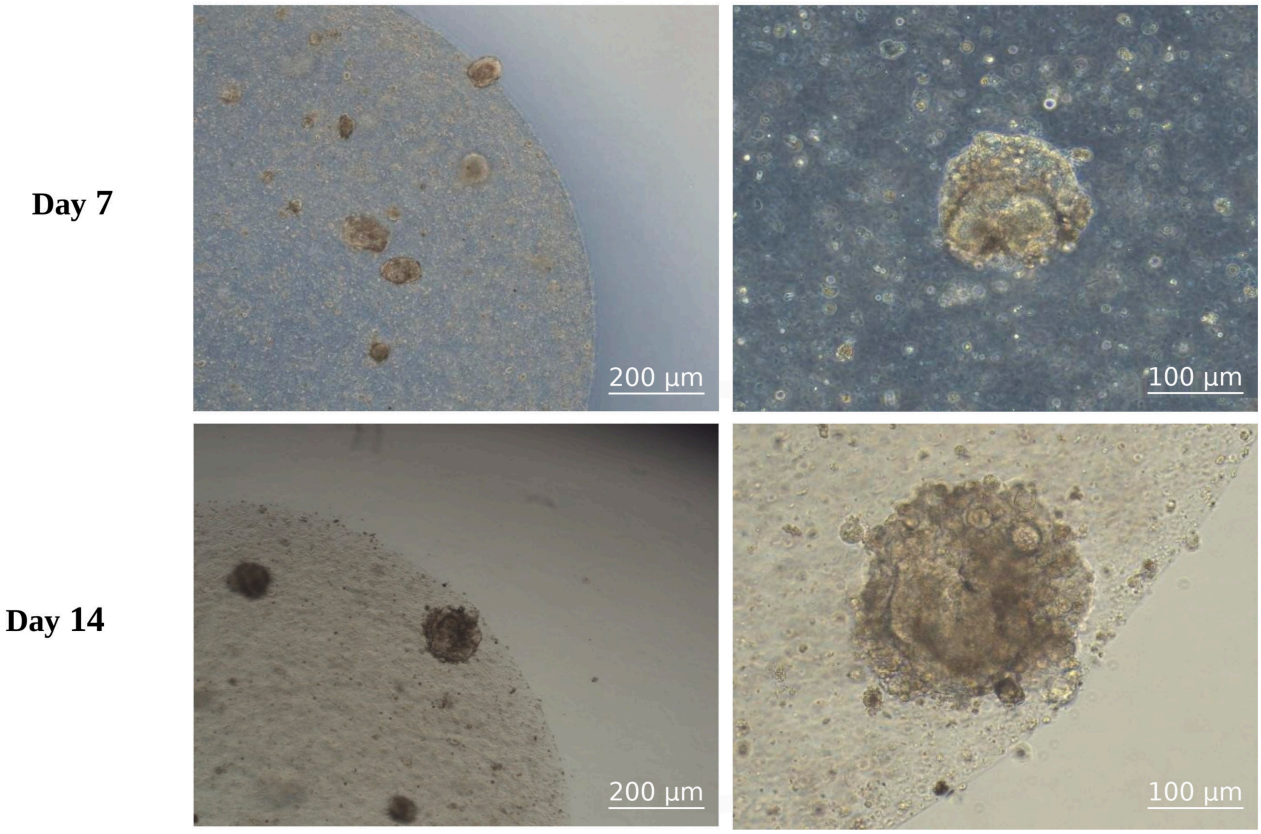

Figure 3. Patient-derived organoids from rectal-origin liver metastasis. Bright-field microscopy images of the organoid lines at day 7 and day 14 of culture. Scale bar: 100 µm, 20× objective; Scale bar: 200 µm, 4× objective).

These observations confirm the capacity of the platform to support rapid establishment and architectural stabilization of tumor-derived organoids suitable for downstream molecular and pharmacologic interrogation.

3.2. Histopathological and Immunophenotypic Concordance with Parental Tumor

Histological comparison between parental liver metastatic tumor tissue and corresponding PDOs demonstrated preservation of key morphological characteristics (Figure 4). Hematoxylin–eosin staining of the primary rectal-origin liver metastasis revealed atypical irregular glandular formations consistent with mucinous adenocarcinoma. The matched organoids displayed peripheral gland-like dense clusters of epithelial organization with pleomorphic nuclei and hyperchromatic features comparable to the original tumor.

Immunohistochemical analysis showed diffuse nuclear p53 positivity in both the parental metastatic tissue and PDO samples, supporting retention of TP53-mutant-associated protein stabilization within the organoid model. The concordant morphologic and immunophenotypic features indicate that the PDO system maintains structural and molecular fidelity relative to the source tumor.

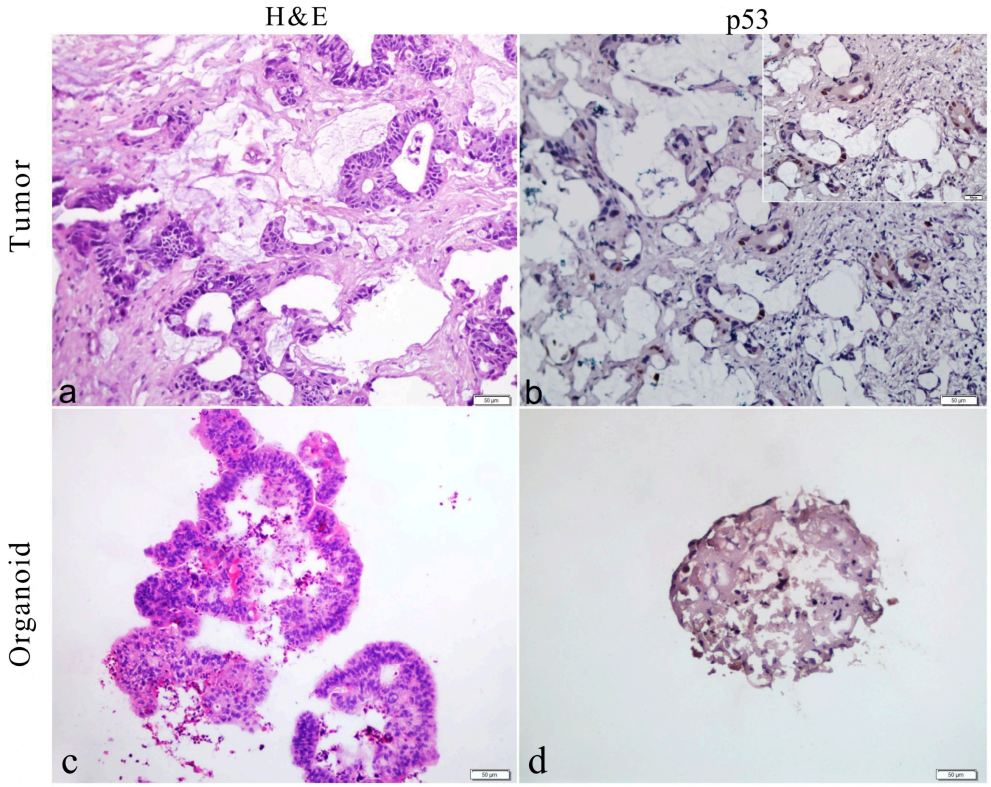

Figure 4. Representative photomicrographs of H&E staining (**a**,**b**) and P53 immunohistochemical staining (**b**,**d**) in patient-derived organoids (PDOs) (**c**,**d**) and corresponding parental rectal tumor tissue (**a**,**b**). Patient-derived rectal cancer organoids reflecting the cellular and histopathological features of the host tissue, including atypical glandular cells, epithelial stratification with H&E staining. Immunohistochemistry shows strong nuclear p53 positivity in glandular epithelial cells of both primary tissue and PDOs (Scale bars: 50 μm, inset: 20 μm).

3.3. Genomic Concordance Between Parental Tumor and Patient-Derived Organoids

To assess the genomic fidelity of the patient-derived organoid relative to its parental tumor, NGS was performed using the NanOnco Plus Panel v3.0 (NanodigmDx, China), which targets the full coding regions of 620 genes relevant to solid tumor biology (including HLA genes), as well as intronic regions associated with common gene fusions, classical microsatellite loci, and chemotherapy-related polymorphisms. In total, 637 genes covering approximately 2.4 Mb of the genome were interrogated, allowing detection of single-nucleotide variants (SNVs), insertions/deletions (indels), copy number variations (CNVs), gene rearrangements, and microsatellite instability (MSI) across a wide genomic spectrum.

A total of 38 tumor-specific variants were identified in the organoid sample; however, the majority represented variants of uncertain significance (VUS) with no established clinical actionability under current ACMG/AMP classification guidelines. Accordingly, six alterations with definite or potential clinical relevance were selected for presentation and downstream interpretation (Table 1), as these constituted the clinically informative subset of the somatic landscape most pertinent to therapeutic decision-making in this case. The KRAS p.A146T (c.436G>A) mutation, previously reported as an activating alteration conferring resistance to anti-EGFR therapies [17,18], represented the sole pathogenic driver mutation of clear clinical significance. Five additional alterations with potential clinical implications were also detected in both patient-derived organoid and its parental tumor. No HER2 amplification or ERBB2 mutation was identified in either the parental tumor or the organoid by targeted NGS, consistent with the absence of HER2 overexpression on immunohistochemistry. These findings were consistent with the molecular landscape of

KRAS/TP53-mutant colorectal carcinomas, in which PTEN loss and CCNE1 amplification have been linked to aggressive biological behavior and therapy resistance [19,20].

Table 1. Clinically relevant somatic alterations detected by targeted NGS in tumor and matched organoid samples.

Gene	Variant/Alteration	Type	Clinical Significance	Detected in
KRAS	p.A146T (c.436G>A)	Missense SNV	Pathogenic	Tumor + Organoid
PTEN	p.C124R (c.370T>C)	Missense SNV	Likely pathogenic	Tumor + Organoid
TP53	p.R175H (c.524G>A)	Missense SNV	Likely pathogenic	Tumor + Organoid
APC	p.Q541fs (c.1620dupA)	Frameshift variant	Likely pathogenic	Tumor + Organoid
APC	p.D1486fs (c.4455delT)	Frameshift variant	Likely pathogenic	Tumor + Organoid
CCNE1	Copy number variation	Gene amplification	Potentially actionable	Tumor + Organoid

The organoid exhibited a TMB of 6.37 mutations/Mb, consistent with a microsatellite-stable profile (microsatellite instability: 6.21%). Importantly, the parental liver metastatic tumor displayed a highly similar genomic architecture, harboring 36 tumor-specific variants, including identical KRAS, PTEN, TP53 and APC mutations as well as the CCNE1 amplification, with microsatellite-stable status and a comparable TMB value of 6.59 mutations/Mb.

The high concordance between the organoid and its originating tumor, including the preservation of all clinically relevant driver events and overall mutational burden, underscores the genetic stability of the organoid system. No additional high-frequency mutations or novel chromosomal aberrations emerged during in vitro expansion. Moreover, copy number variation (CNV) profiling revealed parallel amplification and deletion patterns between the tumor and organoid genomes, particularly in oncogenic loci such as CCNE1 and MYC, while tumor-suppressor regions including TP53 remained heterozygously altered.

Together, these data confirm that the patient-derived organoid faithfully recapitulates the genomic landscape, copy number profile, and mutational burden of the original rectal-origin liver metastasis. This high level of molecular concordance supports its translational utility as an ex vivo precision oncology model for individualized drug sensitivity testing, in line with previous reports demonstrating >60–90% mutational overlap between primary tumors and their derived organoids in gastrointestinal malignancies [21].

3.4. Two-Dimensional Drug Screening Assay

Cells seeded in 384-well plates for 2D culture were exposed individually to each drug in four different concentrations, with three technical replicates per concentration, following a 24 h incubation. To each well, 25 µL of drug solution—diluted in culture medium—was added on top of the pre-seeded 25 µL of cell suspension, resulting in a total volume of 50 µL per well. After 48 h of incubation with the compounds, cell viability was assessed using the Cell Proliferation Reagent WST-1 (Cat#11644807001, Roche Diagnostics GmbH, Mannheim, Germany). WST-1 reagent (5 µL) was added to each well of the 384-well plates and incubated for 3 h at 37 °C in 5% CO_2. Absorbance readings were obtained using a microplate reader (Table 2). Drugs were ranked from the most to the least effective using a proprietary scoring algorithm (CalcuSyn Version 2.0). IC_{50} values were calculated and interpreted in the context of literature benchmarks and ongoing clinical studies. Compounds with significantly lower IC_{50} values were considered "sensitive" and compared with the previously determined "sensitive" hits from the 3D drug screening assay to assess consistency between platforms (Figure 5). Doxorubicin HCl, Carboplatin, and Topotecan were identified as effective agents in the 2D assay, consistent with results obtained from the 3D organoid-based drug screening. This concordance supports the robustness and reliability of our 3D screening results (Figure 6).

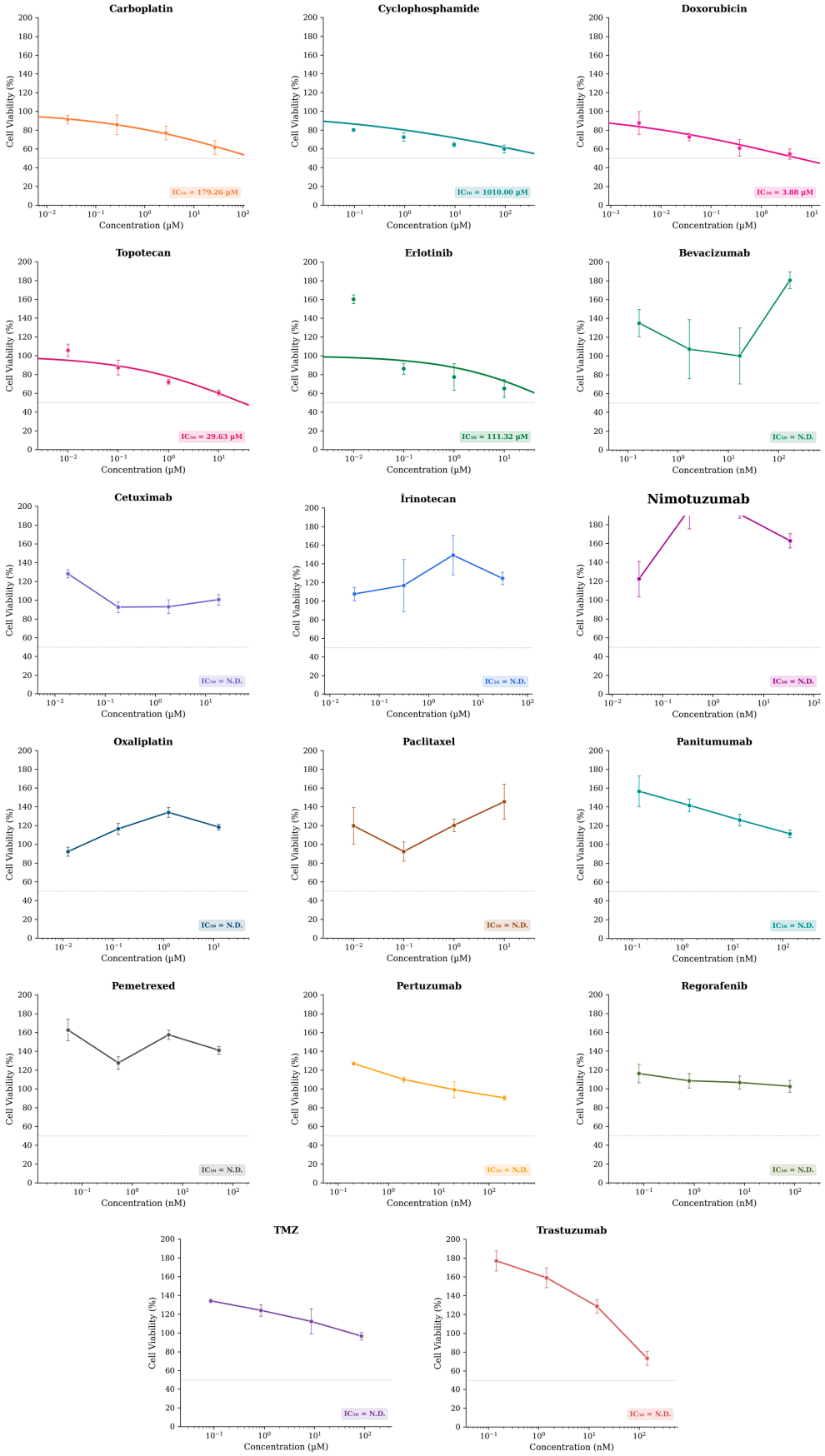

Figure 5. Dose-response profiles of 17 therapeutic agents in 2D monolayer cultures derived from a rectal cancer liver metastasis. Primary cells were seeded in 384-well plates and exposed to four serial

concentrations of each agent for 48 h; viability was assessed by WST-1 assay and expressed as mean ± SD of three technical replicates ($n = 3$) relative to vehicle-treated controls (100%). Curves were fitted by four-parameter logistic (4PL) non-linear regression; curves with $R^2 < 0.90$ were excluded from IC_{50} determination. Five agents yielded quantifiable IC_{50} values: Doxorubicin (3.88 µM), Topotecan (29.63 µM), Erlotinib (111.32 µM), Carboplatin (179.26 µM), and Cyclophosphamide (1010.00 µM). The remaining 12 agents did not achieve ≥50% inhibition within the tested range (IC_{50} = N.D.). N.D. stands for "Not Determined". Concentrations are expressed in µM for cytotoxic agents (carboplatin, cyclophosphamide, doxorubicin, topotecan, erlotinib, cetuximab, irinotecan, oxaliplatin, paclitaxel, temozolomide) and in nM for monoclonal antibody-based agents (bevacizumab, nimotuzumab, panitumumab, pertuzumab, pemetrexed, regorafenib, trastuzumab), reflecting the clinically relevant concentration ranges for each drug class. Resistance to anti-EGFR agents is consistent with the KRAS p.A146T mutation identified in both parental tumor and organoid genomic profiling. Bevacizumab and trastuzumab did not yield quantifiable IC_{50} values in the 2D monolayer system within the tested nM range, consistent with the absence of endothelial components and the mechanism-dependent activity of these agents. Dashed reference line indicates the 50% viability threshold.

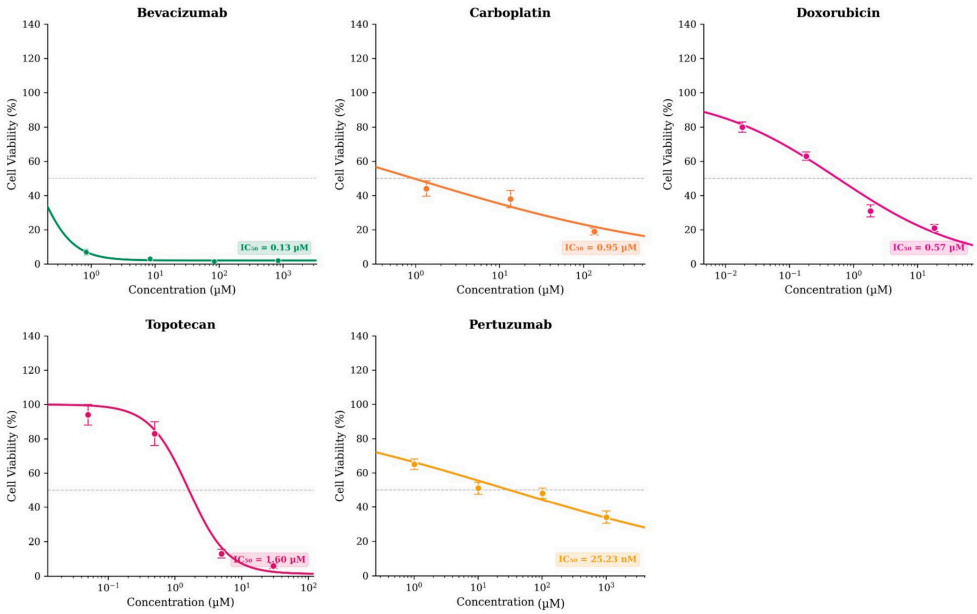

Figure 6. Dose-response profiles of the five therapeutically active agents identified in 3D patient-derived organoid (PDO) drug sensitivity profiling. Organoids were seeded in 384-well plates and exposed to four serial concentrations of each agent for six days; viability was assessed by ATP-based luminescence (CellTiter-Glo®, Promega) and expressed as mean ± SD of three technical replicates ($n = 3$) relative to vehicle-treated controls (100%). Curves were fitted by four-parameter logistic (4PL) non-linear regression; curves with $R^2 < 0.90$ were excluded from IC_{50} determination. Quantifiable IC_{50} values were: Pertuzumab (25.23 nM = 3.73 µg/mL), Bevacizumab (0.13 µM), Doxorubicin (0.57 µM), Carboplatin (0.95 µM), and Topotecan (1.60 µM). The remaining 12 agents did not achieve ≥50% inhibition within the tested range and are not depicted. Dashed reference line indicates the 50% viability threshold.

Table 2. Two-Dimensional WST-1 Drug Screening Results.

Drug	Target	IC_{50} (µM)
Carboplatin	DNA cross-linking agent	179.26
Cyclophosphamide	DNA alkylating agent	1010
Doxorubicin HCl	Topoisomerase II	3.8787
Topotecan	Topoisomerase I	29.63
Erlotinib HCl	EGFR	111.32

Table 2. *Cont.*

Drug	Target	IC_{50} (μM)
Bevacizumab	VEGF-A	NA
Cetuximab	EGFR	NA
Irinotecan HCl	Topoisomerase I	NA
Nimotuzumab	EGFR	NA
Oxaliplatin	DNA cross-linking agent	NA
Paclitaxel	Microtubules	NA
Panitumumab	EGFR	NA
Pemetrexed	Thymidylate synthase	NA
Pertuzumab	HER2	NA
Regorafenib	Multi-kinase inhibitor	NA
Temozolomide	DNA alkylating agent	NA
Trastuzumab	HER2	NA

NA: Not available/applicable; IC_{50} values could not be determined for these agents.

3.5. Three-Dimensional Organoid Seeding for Drug Sensitivity Testing

After a 6-day incubation, 3D organoids seeded in 384-well plates were exposed to each drug at four different concentrations, with three replicates for each concentration. Drugs were prepared in the culture medium, diluted, and applied at 25 μL per well. Drug screening results were evaluated after 6 days of incubation, and CellTiter-Glo® Luminescent Cell Viability Assay (Promega, cat#G7570) was used to measure ATP concentration in the medium as an indicator of cell viability. Results are expressed as mean ± SD of three technical replicates (n = 3) relative to vehicle-treated controls (set to 100%). Data analyses were performed using the GraphPad Prism 7.0b software. Drugs were ranked from the most effective to the least effective using a proprietary metric (CalcuSyn Version 2.0); drugs with IC_{50} values significantly lower than those reported in the literature and active studies were considered "sensitive" and their applicability was evaluated based on the patient's results (Table 3).

Table 3. Tumoroid Chemosensitivity Testing® drug screen results.

Drug	Target	IC_{50} (μM)	Sensitivity	Approved for Indication
Bevacizumab	VEGF-A	0.1300	Sensitive	+
Doxorubicin HCl	Topoisomerase II	0.5700	Sensitive	−
Carboplatin	DNA cross-linking agent	0.9500	Sensitive	−
Topotecan	Topoisomerase I	1.6000	Sensitive	−
Pertuzumab	HER2	0.02523	Low Sensitive	−

Sensitivity classification: Sensitive, organoid IC_{50} below published preclinical reference range; Low Sensitive, IC_{50} within published reference range; Not Sensitive, IC_{50} exceeding reference range or ≥50% inhibition not achieved. "+" means drug is approved for the specific cancer indication being studied. "−" means drug is not approved for the specific cancer indication (though it may be approved for other cancers).

In the Tumoroid Chemosensitivity Test® conducted on the personalized tumor organoids, potential drugs that could provide benefit to the patient were identified as follows: Bevacizumab, by inhibiting VEGF-A and reducing tumor vasculature, can slow the progression of metastatic tumors and potentially enhance the efficacy of existing therapies by modulating the tumor microenvironment. Although organoid systems lack endothelial and stromal components, the observed viability-modulating effect of bevacizumab may reflect tumor-intrinsic autocrine VEGF signaling and VEGF-dependent survival pathways that can be partially preserved in ex vivo tumor models. Accordingly, the IC_{50} value reported for bevacizumab (0.130 μM) should be interpreted as a functional viability-modulating concentration rather than a classical cytotoxic threshold, and caution is war-

ranted in extrapolating this finding to its full anti-angiogenic mechanism in vivo. This mechanism may be particularly beneficial in the liver metastases, which have dense vascular structures. Doxorubicin HCl, by inducing DNA damage, Doxorubicin triggers cell death in cancer cells. When used for localized treatments (e.g., TACE) targeting the liver, side effects may be reduced, and efficacy can be increased [22]. Carboplatin disrupts DNA synthesis, halting cell division, though its effectiveness in colorectal cancer is limited. Its effect can be enhanced in liver metastases through targeted regional applications [23]. Topotecan, by inhibiting DNA replication, Topotecan enhances cell death. It may be beneficial in shrinking liver metastases [24].

Drug sensitivity classification was performed using a three-tiered, literature-anchored framework. For each agent, published preclinical IC_{50} values reported in the same or histologically comparable tumor types were used as reference benchmarks. Compounds yielding an organoid IC_{50} below the published reference range were classified as Sensitive, indicating a response exceeding that documented in the literature context. Compounds whose IC_{50} fell within the reported preclinical concentration range were designated Low Sensitive, reflecting functional activity at pharmacologically achievable concentrations but without exceeding the benchmark threshold. Compounds for which IC_{50} exceeded published reference values, or for which no inhibitory concentration was achieved within the tested range, were classified as Not Sensitive.

Under this framework, Pertuzumab's classification as "Low Sensitive"-despite registering the numerically lowest IC_{50} among all tested agents (25.23 nM; equivalent to approximately 3.73 μg/mL)-is directly attributable to its reference benchmark. Preclinical studies in HER2-positive cancer models employ pertuzumab at working concentrations of 15–20 μg/mL, with clinically relevant Cmax values substantially exceeding 100 μg/mL following standard dosing [25]. Accordingly, the organoid IC_{50} of ~3.73 μg/mL falls within, rather than below, the established preclinical effective concentration range, thereby fulfilling the criteria for Low Sensitive classification. Critically, this tumor harbors no HER2 amplification, ERBB2 mutation, or HER2 protein overexpression; the observed viability-modulating effect most likely reflects low-level baseline HER2 signaling activity rather than biomarker-driven sensitivity. Pertuzumab's clinical utility in this patient would therefore require confirmatory HER2 status assessment and should not be interpreted as a primary therapeutic recommendation in the absence of established HER2 positivity [25] (Figure 6).

To validate the organoid drug-screening findings in a clinically aligned setting, an additional confirmatory assay was performed using trastuzumab deruxtecan (T-DXd), reflecting the patient's current treatment regimen. Bevacizumab was maintained at the previously determined organoid IC_{50} concentration (0.130 μM), and T-DXd was administered at escalating doses (0.001, 0.01, 0.1, 1, and 10 μM). As a single agent, T-DXd demonstrated a dose-dependent reduction in organoid viability across the tested range (Figure 7B), with an IC_{50} of 3.77 μM indicating partial sensitivity. Importantly, when combined with fixed-dose bevacizumab (0.130 μM), T-DXd produced a further downward shift in viability compared with the bevacizumab IC_{50} reference effect and relative to T-DXd monotherapy (Figure 7A), yielding a combination IC_{50} of 0.088 μM. The greatest suppression was observed at higher T-DXd concentrations, supporting an enhanced inhibitory effect of the combination in this patient-derived organoid model.

The exploratory evaluation of T-DXd was further informed by the organoid's sensitivity to topoisomerase I inhibition observed in the primary screening (Section 3.5). Although classical HER2 amplification was absent, the topoisomerase I inhibitor payload of T-DXd may confer cytotoxic activity through a mechanism independent of strict biomarker-defined HER2 positivity, as has been reported in bystander-effect models for antibody–drug conjugates [21]. The clinical observation of disease stabilization under a bevacizumab-containing

regimen at the time of manuscript preparation provides real-world context supporting the translational relevance of these combinatorial findings.

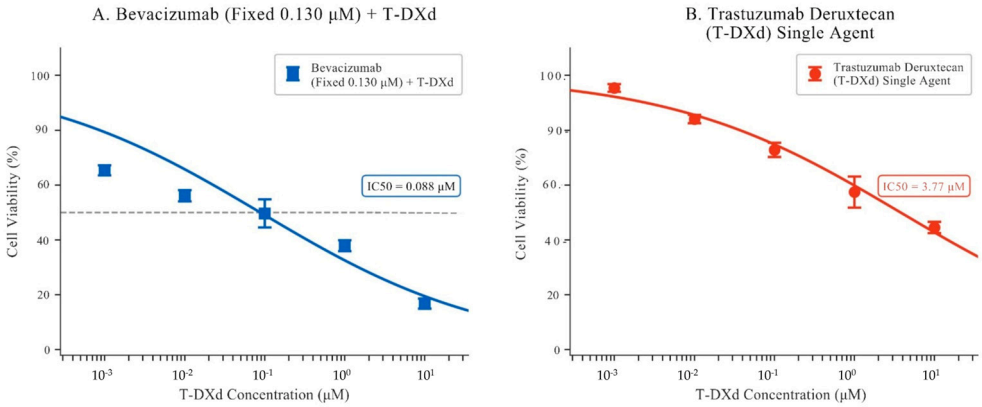

Figure 7. Validation of bevacizumab and trastuzumab deruxtecan (T-DXd) combination in patient-derived organoids. (**A**) Dose-response of T-DXd (0.001–10 μM) in the presence of fixed-dose bevacizumab (0.130 μM; organoid IC_{50}); combination IC_{50} = 0.088 μM. The dashed line denotes the expected bevacizumab IC_{50} reference effect. (**B**) T-DXd single-agent dose-response across the same concentration range; IC_{50} = 3.77 μM. Organoid viability was measured by ATP-based luminescence (CellTiter-Glo®) and normalized to vehicle-treated controls. Data are shown as mean ± SD (n = 3 technical replicates per condition).

These results provide valuable data for a personalized treatment approach beyond conventional chemotherapy and current targeted therapies. Based on the patient's clinical and genetic profile, as well as the organoid-based drug screening and confirmatory validation results, bevacizumab emerged as the highest-ranked therapeutic candidate within the integrated prioritization framework. Given the presence of the KRAS p.A146T mutation, anti-EGFR therapies are expected to be ineffective in this patient. Bevacizumab, which targets tumor vasculature through an anti-angiogenic mechanism independent of EGFR, was identified as the most translationally supported option and may confer an advantage in controlling tumor growth. Bevacizumab is already a widely used and evidence-supported treatment in metastatic colorectal cancer [26]. The remaining identified agents warrant further evaluation through advanced preclinical and clinical studies, ideally within combination therapy regimens, with the aim of improving patient survival and quality of life. In this context, the organoid-based identification of Bevacizumab as the lead candidate—substantiated by both the patient's genomic resistance profile and functional drug screening data—is of considerable translational significance. As described in Section 2.5, a three-dimensional weighted scoring algorithm incorporating IC_{50} magnitude relative to published preclinical reference values, clinical approval status for the relevant indication, and genomic concordance with the patient's molecular profile was applied to support this prioritization; bevacizumab achieved the highest composite score across all three dimensions. The subsequent confirmatory assay (Figure 7) further supports the translational relevance of this prioritization under a regimen aligned with the patient's ongoing clinical management.

It is acknowledged that the present findings derive from a single patient and that patient-specific biological variables—including age (50 years) and sex (female)—may influence organoid pharmacological behavior and, by extension, the broader generalizability of the prioritization outcomes. Specifically, within rectal cancer, sex-based differences in tumor characteristics, treatment response, and survival outcomes have been documented; a large-scale nationwide cohort study of 22,251 rectal adenocarcinoma patients demonstrated that female patients more frequently presented with advanced cT4 tumors and

exhibited distinct survival trajectories compared with male counterparts [27]. Furthermore, sex-related differences in radiosensitivity and chemoradiotherapy toxicity have been specifically reported in advanced rectal cancer, with female patients demonstrating altered normal tissue sensitivity that may reflect underlying differences in drug metabolism and cellular repair capacity [28]. The relevance of these factors to the pharmacological sensitivity profile observed in the present organoid model warrants consideration in future multi-patient validation studies encompassing both sexes and broader age ranges.

4. Discussion

The present proof-of-concept case report demonstrates the feasibility and translational relevance of integrating comprehensive genomic profiling with patient-derived organoid (PDO)-based functional drug sensitivity testing in treatment-refractory rectal cancer liver metastasis. While genomic characterization identified canonical driver alterations (KRASˆA146T, TP53ˆR175H, APC frameshifts, CCNE1 amplification), the absence of high-level actionable biomarkers underscored the therapeutic uncertainty frequently encountered in metastatic colorectal cancer.

Importantly, the PDO model preserved both histopathological architecture and genomic landscape of the parental liver metastatic tissue, including microsatellite stability and low tumor mutational burden. The high concordance observed between tumor tissue and organoid supports the molecular stability of the platform and aligns with prior reports demonstrating substantial mutational overlap in gastrointestinal organoid systems. Preservation of clonal driver events without emergence of dominant culture-acquired alterations further supports the suitability of this system for translational pharmacologic interrogation.

The principal contribution of this case report lies in the functional stratification of therapeutic vulnerabilities beyond biomarker-defined predictions. The organoid-based assay revealed selective sensitivity to bevacizumab, doxorubicin, carboplatin, and topotecan, while anti-EGFR therapies demonstrated limited activity, consistent with the KRAS-mutant genotype. This concordance between genomic resistance markers and ex vivo pharmacologic response highlights the biological coherence of the integrated workflow.

Notably, differential drug potency observed between 2D and 3D platforms underscores the importance of three-dimensional modeling in therapeutic evaluation. The enhanced discriminatory capacity of the organoid system likely reflects preservation of tumor architecture, cell–cell interactions, and survival signaling gradients that are not recapitulated in monolayer cultures. These findings reinforce the concept that functional profiling in structurally relevant 3D systems may refine therapeutic prioritization compared with conventional in vitro assays.

Bevacizumab emerged as the highest-ranked candidate within the weighted prioritization model. It must be acknowledged, however, that organoid systems inherently lack endothelial, stromal, and immune cell components; consequently, the canonical anti-angiogenic mechanism of bevacizumab—blockade of VEGF-A-mediated neovascularization—cannot be fully recapitulated in this ex vivo model. The observed viability-modulating effect is more plausibly attributable to the disruption of autocrine VEGF-dependent survival signaling intrinsic to the tumor epithelial compartment, a phenomenon that has been reported in VEGF-secreting carcinoma cell lines independent of paracrine endothelial interactions. Accordingly, the IC_{50} value derived from the organoid assay should be interpreted as a functional viability-modulating concentration rather than a classical anti-angiogenic threshold, and this mechanistic limitation should be borne in mind when translating these findings to the clinical setting. Notwithstanding these caveats, the convergence of organoid-based sensitivity data with the patient's observed radiological

disease stabilization under a bevacizumab-containing regimen lends meaningful real-world support to the translational relevance of this prioritization.

The patient in this report is a 50-year-old female, and it is pertinent to consider whether biological variables associated with age and sex may have influenced the pharmacological sensitivity profile of the derived organoids. Within the specific context of rectal cancer, sex-based differences in tumor characteristics, neoadjuvant treatment response, and survival outcomes have been documented in large population-based cohorts [27]. Female patients with advanced rectal cancer have furthermore been reported to exhibit distinct radiosensitivity profiles and differential chemoradiotherapy toxicity relative to male patients, findings that may reflect underlying sex-linked variation in drug metabolism and DNA repair capacity [28]. Although PDO systems model the intrinsic molecular pharmacology of the tumor itself rather than systemic pharmacokinetic factors, it cannot be entirely excluded that sex- or age-associated epigenetic or transcriptomic characteristics of the tumor microenvironment have contributed to the sensitivity patterns observed here. Prospective multi-patient studies incorporating matched cohorts stratified by sex and age will be necessary to formally evaluate the influence of these biological variables on organoid-based drug sensitivity profiling in rectal cancer.

The exploratory evaluation of trastuzumab deruxtecan (T-DXd) was informed by the organoid's sensitivity to topoisomerase I inhibition. As confirmed by targeted NGS and immunohistochemistry, this tumor harbors no HER2 amplification, ERBB2 mutation, or HER2 protein overexpression. The observed partial sensitivity to T-DXd in the organoid model is therefore most plausibly attributable to the bystander cytotoxic effect of its topoisomerase I inhibitor payload—a mechanism increasingly recognized as capable of mediating antitumor activity in HER2-low or HER2-negative cell populations in proximity to antibody-targeted cells. This interpretation is consistent with the organoid's independently confirmed sensitivity to topotecan, a topoisomerase I inhibitor, observed in the primary screening. The enhanced inhibitory effect observed for T-DXd under fixed-dose bevacizumab co-treatment further illustrates the capacity of PDO-based combinatorial assays to generate mechanistically informed, hypothesis-guided therapeutic strategies that may not be anticipated from genomic data alone. This interpretation is further supported by preclinical evidence showing that DS-8201a/T-DXd can induce bystander killing in HER2-heterogeneous tumor models, largely attributable to the membrane-permeable nature of its released topoisomerase I inhibitor payload [29].

Collectively, these findings support a functional precision oncology paradigm in which genomic profiling defines the molecular landscape, while organoid-based pharmacologic interrogation refines actionable prioritization. In biomarker-limited, treatment-refractory colorectal cancer, such integrative approaches may help overcome the limitations of genomics-only decision frameworks.

Several limitations should be acknowledged. This proof-of-concept case report represents a single-patient implementation within a broader platform. Organoid systems lack immune, stromal, and vascular components, potentially underrepresenting microenvironment-dependent drug effects. Additionally, prospective clinical correlation across larger and demographically diverse patient cohorts will be required to establish the predictive validity and clinical utility of this integrated platform. Accordingly, the IC_{50} estimates should be interpreted as patient-specific, hypothesis-generating functional readouts rather than biologically replicated efficacy estimates.

Nevertheless, this case report provides a technically integrated and biologically coherent demonstration of a standardized organoid-based functional precision oncology platform. The convergence of histopathologic fidelity, genomic concordance, and pharma-

cologic discrimination supports the translational scalability of this approach for real-time therapeutic prioritization in solid tumors.

Looking ahead, several directions warrant prioritization. First, the integration of immune and stromal co-culture components into the organoid platform would enable more physiologically representative modeling of microenvironment-dependent drug effects, particularly for anti-angiogenic and immunotherapy agents. Second, the application of this workflow to prospective patient cohorts with matched genomic and clinical outcome data will be essential to validate the predictive performance of organoid-derived drug sensitivity profiles in rectal cancer liver metastasis. Third, the development of sex- and age-stratified organoid biobanks from rectal cancer patients would permit systematic investigation of biological variable effects on pharmacological response, addressing a recognized gap in precision oncology evidence. Finally, refinement of the combinatorial drug prioritization framework-incorporating dose-matrix interaction modeling and multi-arm validation-may further enhance the clinical translatability of PDO-based therapeutic recommendations.

5. Conclusions

This proof-of-concept case report demonstrates the feasibility and translational utility of an integrated functional precision oncology platform combining comprehensive genomic profiling with patient-derived organoid-based drug sensitivity testing in treatment-refractory rectal cancer liver metastasis. The established patient-derived organoid model preserved histopathological architecture, key driver mutations (KRASˆA146T, TP53ˆR175H, APC frameshifts, CCNE1 amplification), microsatellite stability, and overall mutational burden of the parental liver metastatic tissue, confirming high genomic and phenotypic fidelity. Functional drug screening identified bevacizumab as the highest-priority therapeutic candidate, corroborated by a weighted scoring algorithm and subsequent combinatorial validation with trastuzumab deruxtecan; the latter agent demonstrated partial single-agent activity and enhanced inhibitory activity in fixed-dose combination with bevacizumab, an effect most plausibly attributable to the bystander cytotoxic activity of its topoisomerase I inhibitor payload in the absence of HER2 amplification. Critically, the patient demonstrated radiological disease stabilization under a bevacizumab-containing regimen, providing real-world clinical support for the organoid-derived predictions. Notwithstanding the inherent limitations of a single-patient implementation, these findings collectively underscore the potential of integrated genomic and ex vivo pharmacologic profiling to guide therapeutic decision-making in biomarker-limited, treatment-resistant metastatic settings, and provide a scalable framework for future prospective validation in larger patient cohorts.

Supplementary Materials: The following supporting information can be downloaded at: https://www.mdpi.com/article/10.3390/organoids5020014/s1. Table S1. Composition of the defined organoid culture medium; Supplementary Methods: Detailed tumor dissociation protocol, 2D and 3D cell seeding procedures, drug preparation and screening conditions, and organoid establishment parameters [16,30]. Table S2. Composition of the 17-agent drug screening panel.

Author Contributions: Conceptualization, B.K.-Y. and M.O.; methodology, E.T.-T., B.K., D.S.-A., A.M.Y. and A.S.; validation, E.T.-T., B.K., A.M.Y., A.S., M.O. and B.K.-Y.; formal analysis, E.T.-T., B.K., K.Y.A., T.B., A.M.Y. and B.K.-Y.; investigation, E.T.-T., B.K., A.M.Y. and A.S.; resources, B.K.-Y., T.B. and M.O.; data curation, M.O.C.; writing—original draft preparation, E.T.-T., B.K., D.S.-A., A.M.Y., A.S. and B.K.-Y.; writing—review and editing, B.K.-Y., D.S.-A., A.M.Y., A.S., T.B., M.O.C. and M.O.; software, K.Y.A. and T.B.; visualization, B.K.-Y. and M.O.; supervision, B.K.-Y.; project administration, B.K.-Y.; funding acquisition, B.K.-Y. All authors have read and agreed to the published version of the manuscript.

Funding: This research was funded by the Scientific Research Projects Coordination Unit of Marmara University (BAPSIS), grant number ADT-2022-10719.

Institutional Review Board Statement: The study was conducted in accordance with the Declaration of Helsinki, and approved by the Institutional Ethics Committee of Marmara University (Approval No: 26-0250; Date: 20 February 2026).

Informed Consent Statement: Written informed consent was obtained from the patient for research use of tumor tissue and for the publication of this paper.

Data Availability Statement: The data presented in this study are available in the article and supplementary material. Additional raw sequencing data and drug screening datasets are available upon request from the corresponding author.

Acknowledgments: The authors would like to express their sincere gratitude to Kamil Yalçın Polat and Gürkan Öztürk from Memorial Bahçelievler Hospital for their invaluable clinical collaboration and for providing the primary tumor tissue specimens essential for this study.

Conflicts of Interest: The authors declare no conflicts of interest.

References

1. Siegel, R.L.; Miller, K.D.; Jemal, A. Cancer statistics, 2019. *CA Cancer J. Clin.* **2019**, *69*, 7–34. [CrossRef]
2. Bray, F.; Laversanne, M.; Sung, H.; Ferlay, J.; Siegel, R.L.; Soerjomataram, I.; Jemal, A. Global cancer statistics 2022: GLOBOCAN estimates of incidence and mortality worldwide for 36 cancers in 185 countries. *CA Cancer J. Clin.* **2024**, *74*, 229–263. [CrossRef]
3. Pinheiro, M.; Moreira, D.N.; Ghidini, M. Colon and rectal cancer: An emergent public health problem. *World J. Gastroenterol.* **2024**, *30*, 644–651. [CrossRef] [PubMed]
4. Bhimani, N.; Wong, G.; Molloy, C.; Pavlakis, N.; Diakos, C.; Clarke, S.; Dieng, M.; Hugh, T. Cost of treating metastatic colorectal cancer: A systematic review. *Public Health* **2022**, *211*, 97–104. [CrossRef]
5. Jafari, A.; Hosseini, F.A.; Jalali, F.S. A systematic review of the economic burden of colorectal cancer. *Health Sci. Rep.* **2024**, *7*, e70002. [CrossRef]
6. Benson, A.B.; Venook, A.P.; Al-Hawary, M.M.; Azad, N.; Chen, Y.-J.; Ciombor, K.K.; Cohen, S.; Cooper, H.S.; Deming, D.; Garrido-Laguna, I.; et al. Rectal Cancer, Version 2.2022, NCCN Clinical Practice Guidelines in Oncology. *J. Natl. Compr. Cancer Netw.* **2022**, *20*, 1139–1167. [CrossRef]
7. Paschke, S.; Jafarov, S.; Staib, L.; Kreuser, E.-D.; Maulbecker-Armstrong, C.; Roitman, M.; Holm, T.; Harris, C.C.; Link, K.-H.; Kornmann, M. Are Colon and Rectal Cancer Two Different Tumor Entities? A Proposal to Abandon the Term Colorectal Cancer. *Int. J. Mol. Sci.* **2018**, *19*, 2577. [CrossRef]
8. Rezaianzadeh, A.; Rahimikazerooni, S.; Khazraei, H.; Tadayon, S.M.K.; Akool, M.A.; Rahimi, M.; Hosseini, S.V. Do clinico-pathologic features of rectal and colon cancer guide us towards distinct malignancies? *J. Gastrointest. Oncol.* **2019**, *10*, 203–208. [CrossRef] [PubMed]
9. Ganesh, K.; Wu, C.; O'rOurke, K.P.; Szeglin, B.C.; Zheng, Y.; Sauvé, C.-E.G.; Adileh, M.; Wasserman, I.; Marco, M.R.; Kim, A.S.; et al. A rectal cancer organoid platform to study individual responses to chemoradiation. *Nat. Med.* **2019**, *25*, 1607–1614. [CrossRef]
10. Costales-Carrera, A.; Fernández-Barral, A.; Bustamante-Madrid, P.; Domínguez, O.; Guerra-Pastrián, L.; Cantero, R.; del Peso, L.; Burgos, A.; Barbáchano, A.; Muñoz, A. Comparative Study of Organoids from Patient-Derived Normal and Tumor Colon and Rectal Tissue. *Cancers* **2020**, *12*, 2302. [CrossRef] [PubMed]
11. Ding, P.; Liska, D.; Tang, P.B.; Shia, J.; Saltz, L.; Goodman, K.; Downey, R.J.; Nash, G.M.; Temple, L.K.; Paty, P.B.; et al. Pulmonary Recurrence Predominates After Combined Modality Therapy for Rectal Cancer. *Ann. Surg.* **2012**, *256*, 111–116. [CrossRef]
12. Nanki, Y.; Chiyoda, T.; Hirasawa, A.; Ookubo, A.; Itoh, M.; Ueno, M.; Akahane, T.; Kameyama, K.; Yamagami, W.; Kataoka, F.; et al. Patient-derived ovarian cancer organoids capture the genomic profiles of primary tumours applicable for drug sensitivity and resistance testing. *Sci. Rep.* **2020**, *10*, 12581. [CrossRef]
13. Al-Aloosi, M.; Prechtl, A.M.; Chatterjee, P.; Bernard, B.; Kemp, C.J.; Rosati, R.; Diaz, R.L.; Appleyard, L.R.; Pereira, S.; Rajewski, A.; et al. Case report: Ex vivo tumor organoid drug testing identifies therapeutic options for stage IV ovarian carcinoma. *Front. Oncol.* **2024**, *13*, 1267650. [CrossRef]
14. Yang, R.; Qi, Y.; Kwan, W.; Du, Y.; Yan, R.; Zang, L.; Yao, X.; Li, C.; Zhu, Z.; Zhang, X.; et al. Paired organoids from primary gastric cancer and lymphatic metastasis are useful for personalized medicine. *J. Transl. Med.* **2024**, *22*, 754. [CrossRef] [PubMed]
15. Hrudka, J.; Fišerová, H.; Jelínková, K.; Matěj, R.; Waldauf, P. Cytokeratin 7 expression as a predictor of an unfavorable prognosis in colorectal carcinoma. *Sci. Rep.* **2021**, *11*, 17863. [CrossRef] [PubMed]

16. Hicks, W.H.; Gattie, L.C.; El Shami, M.; Traylor, J.I.; Davar, D.; Najjar, Y.G.; Richardson, T.E.; McBrayer, S.K.; Abdullah, K.G. Matched three-dimensional organoids and two-dimensional cell lines of melanoma brain metastases mirror response to targeted molecular therapy. *Sci. Rep.* **2024**, *14*, 24843. [CrossRef]
17. Loupakis, F.; Ruzzo, A.; Cremolini, C.; Vincenzi, B.; Salvatore, L.; Santini, D.; Masi, G.; Stasi, I.; Canestrari, E.; Rulli, E.; et al. KRAS codon 61, 146 and BRAF mutations predict resistance to cetuximab plus irinotecan in KRAS codon 12 and 13 wild-type metastatic colorectal cancer. *Br. J. Cancer* **2009**, *101*, 715–721. [CrossRef]
18. De Roock, W.; Claes, B.; Bernasconi, D.; De Schutter, J.; Biesmans, B.; Fountzilas, G.; Kalogeras, K.T.; Kotoula, V.; Papamichael, D.; Laurent-Puig, P.; et al. Effects of KRAS, BRAF, NRAS, and PIK3CA mutations on the efficacy of cetuximab plus chemotherapy in chemotherapy-refractory metastatic colorectal cancer: A retrospective consortium analysis. *Lancet Oncol.* **2010**, *11*, 753–762. [CrossRef]
19. Wang, Z.-H.; Gao, Q.-Y.; Fang, J.-Y. Loss of PTEN expression as a predictor of resistance to anti-EGFR monoclonal therapy in metastatic colorectal cancer: Evidence from retrospective studies. *Cancer Chemother. Pharmacol.* **2012**, *69*, 1647–1655. [CrossRef] [PubMed]
20. Yao, S.; Meric-Bernstam, F.; Hong, D.; Janku, F.; Naing, A.; Piha-Paul, S.A.; Tsimberidou, A.M.; Karp, D.; Subbiah, V.; Yap, T.A.; et al. Clinical characteristics and outcomes of phase I cancer patients with CCNE1 amplification: MD Anderson experiences. *Sci. Rep.* **2022**, *12*, 8701. [CrossRef]
21. Seidlitz, T.; Stange, D.E. Gastrointestinal cancer organoids—Applications in basic and translational cancer research. *Exp. Mol. Med.* **2021**, *53*, 1459–1470. [CrossRef]
22. Sugumar, K.; Stitzel, H.; Wu, V.; Bajor, D.; Chakrabarti, S.; Conces, M.; Henke, L.; Lumish, M.; Mahipal, A.; Mohamed, A.; et al. Outcomes of Hepatic Artery-Based Therapies and Systemic Multiagent Chemotherapy in Unresectable Colorectal Liver Metastases: A Systematic Review and Meta-analysis. *Ann. Surg. Oncol.* **2024**, *31*, 4413–4426. [CrossRef]
23. Osei-Bordom, D.-C.; Kamarajah, S.; Christou, N. Colorectal Cancer, Liver Metastases and Biotherapies. *Biomedicines* **2021**, *9*, 894. [CrossRef]
24. Hackl, C.; Man, S.; Francia, G.; Milsom, C.; Xu, P.; Kerbel, R.S. Metronomic oral topotecan prolongs survival and reduces liver metastasis in improved preclinical orthotopic and adjuvant therapy colon cancer models. *Gut* **2012**, *62*, 259–271. [CrossRef] [PubMed]
25. Xu, Y.; Lv, Y.; Zhu, Z.; Chen, Y.; Zhou, P.; Ye, L.; Tang, W.; Xu, J. Precision medicine in the treatment of colorectal cancer with liver metastases. *Cancer Biol. Med.* **2024**, *20*, 942–946. [CrossRef]
26. Ahn, D.H.; Ridinger, M.; Cannon, T.L.; Mendelsohn, L.; Starr, J.S.; Hubbard, J.M.; Kasi, A.; Barzi, A.; Samuëlsz, E.; Karki, A.; et al. Onvansertib in Combination with Chemotherapy and Bevacizumab in Second-Line Treatment of *KRAS*-Mutant Metastatic Colorectal Cancer: A Single-Arm, Phase II Trial. *J. Clin. Oncol.* **2025**, *43*, 840–851. [CrossRef] [PubMed]
27. Mens, D.M.; van Verschuer, V.M.T.; van Rees, J.M.; Braak, R.R.J.C.v.D.; Verhoef, C.; Hilling, D.E. Nationwide analysis on sex differences in diagnosis, treatment and survival of rectal cancer. *Biol. Sex Differ.* **2026**, *17*, 59. [CrossRef]
28. Schuster, B.; Hecht, M.; Schmidt, M.; Haderlein, M.; Jost, T.; Büttner-Herold, M.; Weber, K.; Denz, A.; Grützmann, R.; Hartmann, A.; et al. Influence of Gender on Radiosensitivity during Radiochemotherapy of Advanced Rectal Cancer. *Cancers* **2022**, *14*, 148. [CrossRef] [PubMed]
29. Ogitani, Y.; Hagihara, K.; Oitate, M.; Naito, H.; Agatsuma, T. Bystander killing effect of DS-8201a, a novel anti-human epidermal growth factor receptor 2 antibody–drug conjugate, in tumors with human epidermal growth factor receptor 2 heterogeneity. *Cancer Sci.* **2016**, *107*, 1039–1046. [CrossRef]
30. Tan, T.; Mouradov, D.; Gibbs, P.; Sieber, O.M. Protocol for generation of and high-throughput drug testing with patient-derived colorectal cancer organoids. *STAR Protoc.* **2024**, *5*, 103090. [CrossRef]

Disclaimer/Publisher's Note: The statements, opinions and data contained in all publications are solely those of the individual author(s) and contributor(s) and not of MDPI and/or the editor(s). MDPI and/or the editor(s) disclaim responsibility for any injury to people or property resulting from any ideas, methods, instructions or products referred to in the content.